Elsevier Editorial System(tm) for Chemical Geology

Manuscript Draft

Manuscript Number:

Title: Unusually Homogeneous Helium Isotope Composition for the Diverse Mantle Sources of the Auckland Volcanic Field

Article Type: Research paper

Keywords: mantle heterogeneity; helium isotopes; trace elements; Zealandia; Gondwana; degassing

Corresponding Author: Dr. Michael Rowe,

Corresponding Author's Institution: University of Auckland

First Author: Michael Rowe

Order of Authors: Michael Rowe; David W Graham; Elaine Smid; Lucy McGee

Abstract: The Auckland Volcanic Field (AVF) is one of the most intensely studied monogenetic basalt fields in the world yet its origin remains enigmatic. Magmatism in the AVF occurred from ~193 ka to 500 ybp and has been variably ascribed to localized heating of lithospheric mantle, tectonic extension and asthenospheric melting associated with the Hauraki Rift. Trace element and isotopic diversity in AVF lavas require three distinct mantle sources, including subduction-modified lithospheric mantle, a fertile garnet-asthenospheric mantle, and a HIMU-like component present as eclogitic/carbonatized mantle (McGee et al., 2013).

Olivine from tephra and lava representing contributions from each of the mantle components, were analyzed for 3He/4He in an attempt to further characterize the AVF "end-members", and to evaluate the potential involvement of a deep hotspot and/or subduction-modified mantle. Olivine grains from tephra were treated with HBF4 to reduce potential contamination from young basaltic glass adhering to olivine grains. Isotopic ratios in 14 samples studied here show a narrow range from 6.57 to 7.26 RA. In comparison, a young arc basalt from the Taupo Volcanic Zone has a significantly lower isotopic ratio of 5.27 RA. The mean 3He/4He ratio of the AVF is 7.10±0.26 RA, consistent with dominance of the helium isotope compositions by the asthenospheric mantle source.

AVF basalts show a negative covariation between the amount of CO2 released by crushing of olivine and the whole rock concentrations of highly incompatible trace elements, such as Ba, Rb, Nb, Zr, Ti and K. In contrast, the amount of He released by crushing shows no simple relations with the same incompatible elements or their ratios, although some positive covariations with Y and middle REE (Tb-Dy-Ho-Er) may relate to the history of magma generation in the presence of garnet at greater depths and lower degrees of melting. These effects lead to a significant variation in CO2/3He ratios (9.4x107 - 3.5x109), with the higher ratios likely to be more representative of the mantle source value. The ~7 RA mantle source for the AVF is consistent with the broader Zealandia-Antarctic mantle domain and the 180 Ma Karoo flood basalts, indicating a

potential tie to initial flood basalt activity and Gondwana break-up in the southern hemisphere. Collectively the results also suggest that the tectonic and magmatic history of the mantle beneath the AVF has effectively hybridized the 3He/4He to a much larger extent compared to other mantle tracers such as highly incompatible trace element ratios and Pb-Nd-Sr isotopes.

Suggested Reviewers: James Scott
University of Otago
james.scott@otago.ac.nz

Matt Jackson
UC Santa Barbara
jackson@geol.ucsb.edu

Takeshi Hanyu
JAMSTEC
hanyut@jamstec.go.jp

Peter Barry
Woods Hole Oceanographic Institute
pbarry@whoi.edu

Research Data Related to this Submission

There are no linked research data sets for this submission. The following reason is given:
All Data is reported in the manuscript body.

Cover Letter

Dear Chemical Geology editor(s),

This manuscript presents new He isotope, and He and CO_2 concentration data, targeting compositional endmembers of Auckland Volcanic Field basalts to understand the mantle heterogeneity underlying the region. This study identifies a mantle component that appears to be related to the larger Zealandia-Antarctic domain and the early break-up of Gondwana and the Karoo Flood basalt superplume. This study also documents the potential influence of melt inclusion vapour bubbles on CO_2/He in olivine separates and demonstrates, interestingly that the basalts thought to originate from a carbonated mantle source, actually have the lowest CO_2 values. In addition, this study presents a methodological comparison between different types of eruptive material (tephra and lava) and a procedure for cleaning samples of groundmass glass opening up a new avenue of potential sample materials for future research.

In total, this manuscript includes 9 figures, 2 tables. The manuscript has a total word count of 8446, including abstract, body, references, and figure captions.

Thank you for your consideration of this manuscript.

Michael Rowe

Unusually Homogeneous Helium Isotope Composition for the Diverse Mantle Sources of the Auckland Volcanic Field

Michael C. Rowe,[1*] David W. Graham[2], Elaine Smid[1], and Lucy McGee[3]

[1]School of Environment, University of Auckland, Auckland 1142, New Zealand

[2]College of Earth, Ocean, and Atmospheric Sciences, Oregon State University, Corvallis, OR 97331, USA

[3]Department of Earth Sciences, School of Physical Sciences, University of Adelaide, Adelaide, Australia

* Corresponding author

Michael Rowe, School of Environment, University of Auckland, Auckland 1142, New Zealand

Email: Michael.rowe@auckland.ac.nz

Tel: +64 9 373 6682

Highlights:

Unusually Homogeneous Helium Isotope Composition for the Diverse Mantle Sources of the Auckland Volcanic Field

ABSTRACT

The Auckland Volcanic Field (AVF) is one of the most intensely studied monogenetic basalt fields in the world yet its origin remains enigmatic. Magmatism in the AVF occurred from ~193 ka to 500 ybp and has been variably ascribed to localized heating of lithospheric mantle, tectonic extension and asthenospheric melting associated with the Hauraki Rift. Trace element and isotopic diversity in AVF lavas require three distinct mantle sources, including subduction-modified lithospheric mantle, a fertile garnet-asthenospheric mantle, and a HIMU-like component present as eclogitic/carbonatized mantle (McGee et al., 2013).

Olivine from tephra and lava representing contributions from each of the mantle components, were analyzed for $^{3}He/^{4}He$ in an attempt to further characterize the AVF "end-members", and to evaluate the potential involvement of a deep hotspot and/or subduction-modified mantle. Olivine grains from tephra were treated with HBF_4 to reduce potential contamination from young basaltic glass adhering to olivine grains. Isotopic ratios in 14 samples studied here show a narrow range from 6.57 to 7.26 R_A. In comparison, a young arc basalt from the Taupo Volcanic Zone has a significantly lower isotopic ratio of 5.27 R_A. The mean $^{3}He/^{4}He$ ratio of the AVF is 7.10±0.26 R_A, consistent with dominance of the helium isotope compositions by the asthenospheric mantle source.

AVF basalts show a negative covariation between the amount of CO_2 released by crushing of olivine and the whole rock concentrations of highly incompatible trace elements, such as Ba, Rb, Nb, Zr, Ti and K. In contrast, the amount of He released by crushing shows no simple relations with the same incompatible elements or their ratios, although some positive covariations with Y and middle REE (Tb-Dy-Ho-Er) may relate to the history of magma generation in the presence of garnet at greater depths and lower degrees of melting. These effects lead to a significant variation in $CO_2/^{3}He$ ratios ($9.4x10^{7} – 3.5x10^{9}$), with the higher ratios likely to be more representative of the mantle source value. The ~7 R_A mantle source for the AVF is consistent with the broader Zealandia-Antarctic mantle domain and the 180 Ma Karoo flood basalts, indicating a potential tie to initial flood basalt activity and Gondwana break-up in the southern hemisphere. Collectively the results also suggest that the tectonic and magmatic history of the mantle beneath the AVF has effectively hybridized the $^{3}He/^{4}He$ to a much larger extent compared to other mantle tracers such as highly incompatible trace element ratios and Pb-Nd-Sr isotopes.

1. INTRODUCTION

Monogenetic basaltic volcanic fields can show a wide range of compositional diversity (Strong and Wolff, 2003; Haase et al., 2008; Nichols et al., 2012; McGee et al., 2013; Rasoazanamparany et al., 2015; Hopkins et al., 2016). The relatively small volume (< 0.1 km^3), and implied lower degree partial melts associated with monogenetic eruptions,

provide an opportunity to investigate mantle processes and materials lost to homogenization in larger magmatic systems (e.g. Stracke and Bourdon, 2009; McGee and Smith, 2016). The geochemical heterogeneity is often ascribed to a multitude of magmatic processes from the mantle through the crust, such as crystal fractionation (Johnson et al., 2008) and melt transport/extraction effects that include melt/wallrock reequilibration or magma mixing (Reiners et al., 1998; Stracke and Bourdon, 2009). However the chemical diversity and the presence of multiple geochemical components, observed both during and between discrete eruptions in a monogenetic field (based on variations in major and trace elements and isotopic abundances) is often beyond what can be reasonably explained by melting of a homogeneous mantle source (Strong and Wolff, 2003). This isotopic and trace element heterogeneity of monogenetic basalts is often cited as evidence of discrete melting of localized mantle heterogeneities (e.g. McGee et al., 2013; Rasoazanamparany et al., 2015; McGee and Smith, 2016).

The Auckland Volcanic Field (AVF; **Fig. 1**), located within the populated city centre of Auckland, New Zealand (population 1.6 million at time of writing), is a monogenetic basaltic field comprised of ~51 eruptive centres with eruption ages from ~193ka to 500 ybp (Leonard et al., 2017). The AVF is arguably one of the world's most intensely studied monogenetic fields (see Determining Volcanic Risk in Auckland (DEVORA) website for compilation of recent publications; www.devora.org.nz). Despite this scientific scrutiny, there is no consensus as to the driving forces of magma generation at depth. Multiple geologic processes have the potential to impact the composition and ascent of AVF magmas locally, including tectonic rifting (e.g. Hauraki Rift; Hodder, 1984), subduction-generated metasomatism (Smith et al., 1993; Huang et al., 2000), and the presence of a mantle "hot zone" (Horspool et al., 2006). The range of AVF basalt compositions supports the idea that one or more of these processes is involved in their magma generation (McGee et al., 2013).

Geochemical modelling of basalt compositions, including whole rock trace element and Pb-Sr-Nd isotope compositions, has led to the explanation that up to 3 distinct mantle sources are present beneath the AVF (McGee et al., 2013; McGee et al., 2015). Magma compositions are, for the most part, highly silica-undersaturated and prior interpretations have suggested they experienced relatively rapid rates of ascent with minimal crustal interaction (McGee et al., 2012; Brenna et al., 2018; Hopkins et al., 2018). Os-isotopic systematics also indicate a minimal amount of crustal interaction, with only marginally elevated $^{187}Os/^{188}Os$ ratios, and no effect on other isotopic or trace element systematics (Hopkins et al., 2016). Predicted end-member magma sources include the lithospheric mantle (having a minor subduction component), garnet-bearing asthenospheric mantle, and an additional source that is variably ascribed to a HIMU-like component generated from melting of ecologitized or carbonatized asthenospheric mantle (McGee et al., 2013; 2015).

Noble gases are key tracers of mantle reservoirs and important for understanding mantle chemical heterogeneity. Changes in noble gas isotopic compositions are also related to processes responsible for U, Th, and K distribution (Graham, 2002). In this study, He isotopic compositions and CO_2 abundances within olivine phenocrysts from the compositional spectrum of AVF basaltic magmas have been measured to assess the possible variations in source compositions and potential metasomatic effects. This new data provides important insight into the source history of the wider New Zealand mantle, with implications for where and why AVF magmas are generated.

2. METHODS

2a. Sample Selection

Twelve samples were selected from eight Auckland volcanic field centres to cover the compositional range of potential mantle sources described by McGee et al (2013) (Table 1).

Most samples were fresh tephra containing olivine phenocrysts that were then separated by hand-picking under a binocular microscope. Three lava samples were also analysed for comparison, including a basaltic lava from the Taupo volcanic zone (Ongaroto, Onga-1; Table 2). A complete list of AVF samples and locations is available in Table 1. Samples designated with an "AU" prefix originate from the University of Auckland sample archive. Volcano names are all provided in Te Reo Maori.

2b. Olivine Preparation

For lava samples (Rangitoto, Maugarei, and Ongaroto), blocks were lightly crushed and olivine grains were manually separated. Grains were relatively clean, unaltered and free of adhering groundmass. Tephra samples were first sieved to identify loose olivine crystals, then clasts were very lightly crushed to disaggregate tephra. Olivine phenocrysts were hand-picked under a binocular microscope from both tephra and lava samples. Clean samples (lacking glass or alteration on grain exteriors) primarily came from the lava samples. Tephra olivine samples included varying and significant amounts of glass adhering to grain surfaces. Tephra olivine was treated in fluoroboric acid (HBF_4) at the University of Oregon to remove adhering glass. Grains were placed in small plastic beakers and covered with HBF_4. Time in the HBF_4 ranged between 30 minutes and 1 hour. Samples were swirled lightly every 15 minutes. Small grains were limited to 30 minutes while time for larger grains or grains with significant glass varied to optimize removal of exterior glass while reducing etching to grain surfaces. Despite the relatively short duration in HBF_4, treated olivine grains were generally more brittle than untreated grains, and usually showed a decrease in mean grain size (**Fig. 2**). After leaching, the samples were neutralized with Na_2CO_3 and then rinsed with water and isopropanol. All samples underwent a series of Ethanol washes in an ultrasonic bath in 5-10 minute increments to remove any remaining unwanted debris, with re-checking/picking for a comprehensive removal of all surface coatings on grains. Final sample weights ranged from

0.0709g to 0.4333g (mean size was 0.1357 g). Two of the samples were also analysed without leaching, to provide a test of the effects of adhering glass on the measured $^{3}He/^{4}He$ ratio and the He and CO_2 concentrations.

2c. Isotope Measurements

Helium abundance and isotopic measurements on olivine were performed at Oregon State University following established methods (Graham et al., 2014). Individual samples were crushed in vacuum to extract gases trapped in fluid and/or melt inclusions within the mineral grains. CO_2 was isolated during the crushing using a liquid nitrogen cold trap, and its concentration was subsequently determined by capacitance manometry (Graham et al., 2018). He concentrations were determined by comparison of peak heights to a calibrated helium standard. Line blanks were performed before sample analyses; the average ^{4}He blank was 2.7 x 10^{-11} ccSTP ^{4}He, and comprised between only 0.1 to 3.9% of the ^{4}He measured in the AVF sample suite (with the exception of olivine from the Taupo Volcanic Zone Ongarato basalt, for which it was 7%). All the reported helium isotope results in this study are blank corrected.

2d. Trace Elements Analysis

Whole rock major and trace element abundances for nine samples were measured at Washington State University following routine procedures for sample preparation and analysis via XRF and ICPMS (Johnson et al., 1999; Knaack et al., 1994). These analyses are augmented with 3 further analyses of samples AU62410; AU62438, and AU62444, from McGee (2012), covering the spectrum of proposed end-member compositions (Table 1).

3. RESULTS

Whole rock major and trace element abundances for the tephra and lava samples are reported in Table 1. Incompatible trace element abundances show nearly an order of magnitude variation. The sub-alkaline Rangitoto lava and tephra are distinct outliers

compared to the other alkaline, silica-undersaturated basaltic samples (**Fig. 3**). Collectively, alkaline tephras and lavas have similar trace element and REE patterns, albeit with varying degrees of enrichment at similar MgO contents. The alkaline magmas are characterized by a distinctive enrichment in Nb and Ta and a marked depletion in K, and although variable, a relative depletion in Pb (**Fig. 3a**). REE distribution is used here to categorize the basalts for later discussion (**Fig. 3b**). For example, the $La/Yb_{[N]}$ ratio can be affected both by the presence of garnet during melting (due to compatible behaviour of HREEs) and by varying source enrichment, and degree of melting, (which more strongly leverages variation in LREEs). Subalkaline magmas in the AVF have characteristically low $La/Yb_{[N]}$ of ~5, while alkaline magmas have $La/Yb_{[N]}$ between 13-35. The alkaline magmas can be further subdivided, with $La/Yb_{[N]}$ forming two main clusters from ~13-15 and ~28-35, with several transitional samples having $La/Yb_{[N]}$ of ~19-22. These groupings are consistent with the prior source trace element modelling by McGee et al (2013). McGee et al (2013) showed that REE partial melt + mixing suggests that a $La/Yb_{[N]}$ of greater than ~20 and a $Gd/Yb_{[N]}$ greater than ~4.0 required an asthenospheric component contaminated with ecologitic material, with lower $La/Yb_{[N]}$ and $Gd/Yb_{[N]}$ indicative of mixing between lithospheric (subduction-influenced) and fertile asthenospheric mantle.

New CO_2 and He results are reported in Table 2. The He concentrations in olivine from the Auckland volcanic field range from 1.8 $x10^{-7}$ to 1.1 x 10^{-8} cm^3 STP/g (Fig. 4). Despite the order of magnitude variation in [He], $^3He/^4He$ ratios (R_A) for the 14 samples lies in a very narrow range from 6.6 to 7.5 (mean = 7.10 +/- 0.26; Fig. 4). Replicate analyses (HBF_4-treated and untreated) of the Rangitoto volcano tephra showed no systematic effect on $^3He/^4He$ between leached (to remove adhering glass) and unleached analyses (**Fig. 5**). Sample AU49951 has an identical $^3He/^4He$ of 7.26 R_A, regardless of treatment, but slightly different He concentrations of 9.8$x10^{-8}$ cm^3 STP/g(treated) vs, 1.3 x 10^{-7} cm^3 STP/g (untreated). In

contrast, Sample AU59337 has a $^{3}He/^{4}He$ of 6.79 +/- 0.18 R_A (untreated) vs. 7.15 +/- 0.16 R_A (treated). In this case, the untreated sample had a significantly higher sample mass and lower He concentration (3.2 x 10^{-8} cm^3 STP/g) compared to the treated sample (1.1 x 10^{-7} cm^3 STP/gHe). Sample heterogeneity due to a varying amount of fluid/melt inclusions trapped in olivine may be a possible explanation for this difference. The results may also indicate that the presence of excess surficial (and highly degassed) glass in sample AU59337 led to a lower measured He concentration, with a slightly lower $^{3}He/^{4}He$ due to a larger component of post-eruptive radiogenic helium that was present from alpha-implantation into the outer surface of the olivine grains. More work is needed to distinguish between these possibilities.

In addition to the treated-untreated comparison, our results allow a comparison between co-existing lava and tephra samples (Fig. 5). Treated olivine from tephra AU59337 compared to co-existing subalkaline lava (Rangi-1) have indistinguishable $^{3}He/^{4}He$ ratios of 7.15 +/- 0.16 R_A and 7.02 +/- 0.16 R_A, respectively. The Maungarei tephra (078) and lava (AU62410) show a slight offset in $^{3}He/^{4}He$, but nonetheless have similar values (7.08 +/- 0.17 R_A and 6.72 +/- 0.23 R_A, respectively). Helium abundances are systematically higher in olivine from tephra samples compared to those from lava flows. Although the results are somewhat variable, they suggest that leaching of glass-coated olivine from tephra in HBF_4 helps to increase the yield of He (cm^3 STP/g) when significant exterior glass is present, and may result in slightly higher measured $^{3}He/^{4}He$ ratios (Fig. 5). Although an appreciable difference in $^{3}He/^{4}He$ between lava and co-genetic tephra is absent, the He concentration yields appear to be significantly elevated for treated tephra olivine compared to untreated olivine from lava flows that has minimal adhering groundmass. For consistency, going forward we only incorporate treated, or glass-free, tephra and lava olivine separates.

Similar to He, CO_2 abundances vary by an order of magnitude, ranging from 1.3 x 10^{-4} to 2.1 x 10^{-3} cm^3 STP/g (**Table 2**). As noted in Table 2, when our measured pCO_2 is <1

mtorr, analytical uncertainties are generally significantly larger. In addition, CO_2 concentrations are not available for untreated tephra samples because in these cases the pCO_2 was near the detection limit (≤0.2 mtorr). The measured [CO_2] in olivine from the Maungarei lava (AU62410, 0.0056 cc/g) is 2.5 times lower than in the coexisting tephra (078, 0.0014 cc/g; Fig. 5). This result is consistent with the relative depletion in [He] measured in these two samples. In contrast, despite the enrichment in [He] for olivine from the Rangitoto tephra (AU59337) relative to the lava-hosted olivine (MR-Rangi1), the [CO_2] is depleted by nearly a factor of 2. In general, [CO_2] is not correlated to [He] or $^3He/^4He$.

Neither the isotopic composition nor abundance of He is correlated with the whole rock chemical or Sr-Nd-Pb isotopic compositions (Fig. 6a-b; McGee et al., 2013). However, CO_2 abundances are negatively correlated with whole rock incompatible trace elements, excluding HREEs (Fig. 6c-f). The range of CO_2/He ratios in all samples varies from $9.4x10^2$ to $6.4x10^4$ ($9.4x10^7$ to $6.4x10^9$ for $CO_2/^3He$ respectively) and shows no correlation with $^3He/^4He$ (Fig. 7). There does appear to be a weak correlation between $CO_2/^3He$ and $La/Yb_{[N]}$, however it is driven almost entirely by the variation in olivine [CO_2] (Fig. 7).

4. DISCUSSION

4a. Implications of [CO_2] and [He] variations

As described above, La/Yb is a useful discriminant for magmatic end-members and their mantle sources (McGee et al., 2013). Although the He concentrations in olivine show no correlation with major or trace elements, CO_2 concentrations are negatively correlated with La/Yb (**Fig. 7**). Trapped [CO_2] in olivine of subalkaline samples lies between 0.0012 to 0.0021 cm^3/g (2.4 to 4.1 ppm CO_2) while in alkaline samples it shows lower values and a larger range, between 0.00013 to 0.0014 cm^3/g (0.3 to 2.8 ppm CO_2). These variations in the amount of trapped CO_2 and He in olivine depend on 1) differences in sample preparation, 2)

mineral grain properties (size, cleavage, etc.), and 3) magmatic processes (extent of crystal fractionation, volatile degassing, etc.).

In terms of sample preparation, we are primarily concerned with the effect of the HBF_4 treatment used to remove volcanic glass that coats olivine grains in tephra. Despite the young age of erupted basalts (<193 ka; Leonard et al., 2017), the high abundances of U and Th (up to 3 ppm and 10.8 ppm, respectively) make the initial amount of trapped magmatic He and its isotopic compositions potentially susceptible to contamination by post-eruptive radiogenic ^{4}He. Assuming a minimum mass proportion of 10% degassed glass was present for our olivine mineral separates, closed system post-eruptive production of ^{4}He would result in a decrease in ^{3}He/^{4}He of < 0.1 R_A given the measured amounts of ^{4}He that were released by crushing. The one exception is the Lake Pupuke sample (discussed below). This small offset of < 0.1 R_A is consistent with the results for treated versus untreated samples (**Fig. 5A**) and is generally comparable to the analytical uncertainty in the ^{3}He/^{4}He measurement. In contrast, for the oldest sample (Lake Pupuke, 193 ka; Leonard et al., 2017), 10% contamination by post-eruptive radiogenic helium from adhering glass would lead to the addition of 1.6×10^{-8} cm^3/g ^{4}He and a potential downward shift in ^{3}He/^{4}He by 1.6 R_A. Depending on the amount of magmatic helium that was trapped in the olivine, volcanic glass coating this sample may constitute a more significant proportion by mass. Therefore the HBF_4 cleaning procedure is recommended for glass-coated tephra in somewhat older samples such as this one. Furthermore, there is no evidence to suggest this procedure affects the abundance of gas for analysis (i.e., there was no preferential leaching of gas trapped in fluid/melt inclusions) (**Fig. 5b**). Therefore we look to natural processes to explain the CO_2 and He variations.

The anti-correlation between whole rock trace elements (e.g. U, La, Zr) and ratios (e.g., La/Yb) and trapped CO_2 content of olivine, and by extension CO_2/^{3}He, suggest the

involvement of a magmatic process or a mantle source control (**Fig. 6, 7**). High-La/Yb_N alkali basalts in the AVF have been proposed to originate as low-degree (<1%) partial melts compared to the subalkaline magmas originating from ~3% partial melting (McGee et al., 2013). Thus, the trapped CO_2 content of olivine should vary inversely with the degree of melting, due to its incompatibility. This behaviour is opposite to what is observed (Fig. **7c**), and what would be expected if the mantle source of both alkaline and subalkaline basalts had the same concentration of carbon, and if magmatic CO_2 was controlled by the degree of melting in the same way as La/Yb.

Differences in the mode of degassing during magma ascent can lead to fractionation of $CO_2/^3He$ in magmatic systems (e.g., Tucker et al., 2018). Fractionation of $CO_2/^3He$ may result from the higher solubility of He compared to CO_2 during equilibrium, closed system degassing (Tucker et al., 2018; Graham et al., 2018). Open system degassing (such as Rayleigh distillation) will significantly enhance this $CO_2/^3He$ fractionation. For example, a large extent of Rayleigh degassing (99%) will leave a residual magma with a $CO_2/^3He$ ratio that is 10 times less than its original value (Horton et al., 2019). In contrast to equilibrium degassing, kinetic fractionation favours He loss, because the high diffusivity of helium in the melt leads to equilibrium vapor/melt partitioning for helium, while the much lower diffusivity of CO_2 in the melt leads to vapor/melt disequilibrium). Depending on magma ascent rate, kinetic fractionation might therefore mitigate the effects of differing CO_2 and He solubilities during equilibrium degassing. Open-system Rayleigh degassing is likely to be more common in slowly ascending magma, or during protracted stalling and storage in the crust, and lead to more efficient separation of the gas phase from melt. In order for degassing to significantly impact the CO_2-trace element correlations, a secondary control such as magma ascent rate must be involved. However, the CO_2-La/Yb correlation is opposite of what would be expected, because lower degree melts (having higher abundances of trace elements and

volatiles) would be expected to have lower viscosity and therefore should ascend more rapidly compared to the higher degree subalkaline melts (having relatively lower abundances of trace elements and volatiles) that may slow their ascent or stall in the crust.

In olivine, gas concentrations and potentially the ratios of volatile elements depend on the ability of olivine to trap both melt and vapour phases. The variations in He and CO_2 concentration measured by crushing of AVF olivines could be controlled by volatile exsolution into vapour (shrinkage) bubbles after melt inclusion entrapment (**Fig. 8**), or it could be controlled by the amount of fluid trapped from a vapour-saturated melt. Recent studies have highlighted the significance of gas (CO_2) in vapour shrinkage bubbles associated with melt inclusions (Moore et al., 2015; Tucker et al., 2019). Measurements of shrinkage bubble volumes from Hawaiian volcanoes show a maximum frequency at only 3-4 vol.% (predominantly less than 8 vol.%), but there are some outliers at >20 vol.% (Tucker et al., 2019). CO_2 density in shrinkage bubbles can vary significantly, from 0.04 to 0.5 g/cm^3 (Moore et al., 2015; Aster et al., 2016; Tucker et al., 2019) based on both equation of state (EOS) calculations and Raman spectroscopy measurements. In contrast, fluid inclusions trapped directly from vapour-saturated melt tend to have higher CO_2 densities in high pressure mafic crystalline phases, with densities ranging from 0.2-1.13 g/cm^3 (Hidas et al., 2010; Schwab and Freisleben, 1988). Therefore, the volume proportion of shrinkage bubbles in melt inclusions relative to trapped fluid inclusions may be a factor in controlling the CO_2/He ratio measured by crushing olivine mineral separates.

Given the lower solubility of CO_2 compared to He in basaltic melts (Tucker et al., 2018; Graham et al., 2018), a system closed to CO_2 loss such as a melt inclusion may undergo CO_2/He fractionation following entrapment and formation of shrinkage bubbles. This should lead to a higher CO_2/He in the gas phase compared to dissolved in the melt inclusion. Kinetic fractionation might produce an opposing effect on the CO_2/He ratio, but in

this case this depends on the relative diffusion rates of He and CO_2 compared to the cooling / quenching rate of the melt inclusion. To quantitatively characterize the role of shrinkage bubbles in melt inclusions relative to directly trapped fluid inclusions would require a knowledge of the shrinkage bubble and fluid inclusion volumes, the relative densities of CO_2 and He, and the distribution of the inclusions through a bulk olivine separate. Based on X-ray computed tomography coupled with single crystal gas analysis for CO_2 and He in Samoan olivines, Horton et al (2019) argued that He is primarily stored in fluid inclusions. However, melt inclusions were not taken into account in that study due to limitations in image resolution. Notably, He concentration correlated broadly with fluid inclusion density but CO_2 concentration was uncorrelated in the Horton et al (2019) study, suggesting that there may have been a secondary CO_2 source.

Too many unknowns exist to constrain these parameters in our study, but we can theoretically consider the impact of post-entrapment crystallization on CO_2 abundances. The primary observation is that CO_2 concentrations correlate with whole rock incompatible trace elements and LREE/HREE while He concentrations do not. A priori one expects that slower magma ascent rates following olivine crystallization at depth would lead to more CO_2 exsolved into melt inclusion shrinkage bubbles (**Fig. 8**). The degree of trace element enrichment in the magma (**Fig. 3, 6**) might also be proportional to magma ascent rate, given that higher degree partial melts (subalkaline magmas) are expected to ascend more slowly. This combination of factors is quite plausible, but it requires basic assumptions about the relative differences in magma ascent rate for different magma types, and its effect on the amount of CO_2 and He trapped in melt inclusion shrinkage bubbles.

Despite the potential complications of magma sources and degassing models, one consequence of the early enrichment of CO_2 in small degree partial melts is that the onset of CO_2 saturation occurs deeper/earlier (**Fig. 8**). This early saturation can lead to more

significant early degassing of a CO_2-rich volatile phase and thus, counterintuitively, low degree melts may end up with lower CO_2 abundances at the time of olivine crystallization relative to higher degree partial melts (e.g. Gonnermann and Mukhopadhyay, 2007). Early saturation of a CO_2-rich volatile phase should also result in greater degassing of helium. Although the He concentrations show a comparable range of variability to the CO_2 concentrations in our study (14x versus 16x), the absence of correlation between the volatile phases might result from a more rapid (compared to CO_2) re-equilibration of He with host melts after olivine crystallization (Horton et al., 2019). Post-entrapment kinetic fractionation could also favour diffusive loss of He from olivine and therefore, in many instances, the measured $CO_2/^3He$ ratio trapped in olivine-hosted inclusions may not represent the original melt ratio (Horton et al, 2019). Notably, despite more than an order of magnitude variation in olivine trapped helium content, there is no correlation of He concentration with whole rock chemistry (F**ig. 6**); the larger variation in CO_2 contents is what drives the correlation between La/Yb_N and $CO_2/^3He$ (**Fig. 7**). Although we cannot quantitatively evaluate the potential diffusive loss of He after entrapment, we note that the similar olivine He concentrations in lava and tephra from the same volcano shown in **Fig. 5** (which are associated with dramatically different cooling rates) suggest that any post-entrapment re-equilibration of He seems to have mostly occurred prior to eruption. Therefore, the inverse relationship between CO_2 and La/Yb_N likely reflects the effects of early CO_2 saturation and volatile exsolution (**Fig. 8**), while the trapped He content of olivine (which is uncorrelated with CO_2 and whole rock trace elements) is primarily controlled by its more rapid re-equilibration with the host magma during its transport through the crust. Interestingly, this means that the smallest volcanic centres, thought to be derived from a carbonated mantle domain (McGee et al., 2015), counterintuitively retain the lowest CO_2 abundances.

4b. Significance of $^3He/^4He$ to the Origin of the AVF

As noted above, $^{3}He/^{4}He$ isotopic values of Auckland Volcanic Field magmas preserve a homogeneous composition, of 7.10 ± 0.25 R_A, despite major- and trace-element compositional differences (Fig. 3, 4, 6). Prior analyses of 3 different volcanoes/samples in the AVF (Wiri, Puketutu, and Crater Hill) indicate a wider range in composition but still maintain a similar average of 7.28 RA (Fig. 9; Patterson et al., 1994). Crustal interaction, particularly for the alkaline magmas, appears to be limited, with low $^{187}Os/^{188}Os$ (indicating less the 1%; Hopkins et al., 2016) and an olivine $\delta^{18}O$ of 5.3 ± 0.6 (Coote et al., 2019) for the Auckland Volcanic Field. Ascent rate models for AVF magmas from trace element and hydrogen diffusion in xenocrystic mantle olivine suggest relatively long residence times in the mantle (up to a year), followed by relatively rapid (< week) ascent through the crust (Brenna et al., 2018). The absence of prolonged crustal storage for AVF magmas would reduce the likelihood of significant crustal contamination.

Any attempt to account for the He isotope composition of the mantle underlying the Auckland volcanic field must address the key observation that it has low (~7 R_A) and uniform $^{3}He/^{4}He$, despite the trace element and isotopic heterogeneity observed in the AVF basalts (McGee et al., 2013). This He isotope composition, lies at the boundary between most MORB (7-10 R_A) and most lavas and xenoliths derived from the sub-continental lithospheric mantle (SCLM 5-7 R_A; Porcelli et al., 1992; Reid and Graham, 1996; Gautheron and Moreira, 2002; Dunai and Porcelli, 2002). Given the complex tectonic history of New Zealand over the last ~100 my (e.g. Jiao et al., 2014; Seebeck et al., 2014), it is not unreasonable to assume potential metasomatic enrichment in the upper mantle, either from intra-mantle trapped melts or subduction modification as the source of slightly more radiogenic He isotope compositions compared to depleted mantle. In addition to Mesozoic subduction and accretion events responsible for the construction of Zealandia (e.g. Jiao et al., 2014), tectonic models suggest the upper mantle beneath the AVF could have experienced subduction-derived metasomatism

from 30-15 Ma (Haung et al., 2000), and as recently as 8 Ma (Seebeck et al., 2014). The He isotopic range in subduction-related magmas has long been explained as a mixture between MORB-like He ($^3He/^4He$ = 7-10 R_A) and radiogenic He (<0.1 R_A) derived from the crust or lithosphere (e.g. Poreda and Craig, 1989; Porcelli et al., 1992; Hoke et al., 2000; Hilton et al., 2002). Notably, young subduction-derived basalts of the Taupo Volcanic Zone, including a new analysis at 5.7 ± 0.27 R_A, have systematically lower $^3He/^4He$ of 5.7 +/- 0.8 R_A (**Fig. 9**; Patterson et al., 1994) compared to the AVF, and are similar to the global arc mean of 5.4 +/- 1.9 R_A (Hilton et al., 2002).

Prior trace element and isotopic (Sr-Nd-Pb) modelling suggested a significant role for the shallow upper mantle (up to 80% subduction-modified spinel lherzolite), particularly in the generation of higher degree partial melt basalts, such as Rangitoto volcano subalkaline compositions (McGee et al., 2013). Only a very weak enrichment of fluid mobile trace elements is evident in AVF subalkaline basalts compared to alkaline ones, with average Ba/Nb and U/Nb at 7 and 0.033, and 5 and 0.024, respectively (**Fig. 3**). Despite the potentially significant role for a compositionally distinctive, metasomatised shallow upper mantle in the generation of the AVF basalts, subalkaline He-isotope compositions (treated-tephra and lava) range only from 7.02 to 7.16 R_A, just overlapping with the least radiogenic values observed in volcanic arcs globally (Hilton et al., 2002). However, the AVF alkaline magmas, interpreted as distinctly deeper, lower-degree partial melts (McGee et al., 2013), have identical $^3He/^4He$. While a slight influence from subduction-related processes is possible for the subalkaline magmas based on $^{87}Sr/^{86}Sr$ and fluid-mobile trace element enrichments, such enrichments are absent in the alkaline magmas. Subduction-related metasomatism of the upper mantle therefore cannot readily account for the uniform $^3He/^4He$ amongst the range of AVF magma compositions. A low-velocity seismic anomaly at ~80-100 km depth beneath the AVF suggests the presence of a localized thermal or compositional anomaly (Horspool et

al., 2006). Although it is unclear from the available data if this low-velocity zone extends to greater depth, the absence of $^{3}He/^{4}He$ above ~10 R_A in the AVF indicates that its mantle source contains an insignificant contribution from deeply derived, relatively high $^{3}He/^{4}He$ plume material (e.g. Kurz et al., 1982).

New Zealand resides within the so-called HIMU province of the SW Pacific (e.g. Woodhead, 1996, Panter et al., 2006; McCoy-West et al., 2010; Scott et al., 2014), more recently designated as the "Zealandia-Antarctic" mantle domain (Park et al., 2019). The domain is isotopically characterized by mixing between HIMU- FOZO- EMI-EMII mantle endmembers (Hart et al., 1992; Finn et al., 2005). Studies have long debated the origin of this domain, and in particular the HIMU component, and primarily have suggested either a sub-continental lithospheric mantle (SCLM) or a sub-lithospheric source (e.g. Panter et al., 2006; McCoy-West et al., 2010; Scott et al., 2014; Park et al., 2019). HIMU basalts have characteristically elevated $^{206}Pb/^{204}Pb$ compared to other ocean island basalts due to a time-integrated elevated U/Pb ratio in the mantle source. HIMU basalts also have low $^{3}He/^{4}He$ ratios that overlap with the low end of the range in typical mid-ocean ridge basalts derived from the upper mantle (~5.8-7.0 R_A: Graham et al., 1992; Hanyu et al., 1997; 2014), consistent with a mantle source that also has elevated (U+Th)/He. Despite the AVF $^{3}He/^{4}He$ ratios of ~7 R_A in AVF lava and tephra that have OIB-like trace element concentrations, and the prevalence of HIMU basalts throughout the SW Pacific that include the South Island of New Zealand (e.g. Hoke et al., 2000; McCoy-West et al., 2010), these young AVF basalts lack the characteristic $^{206}Pb/^{204}Pb$ enrichment of HIMU domains (McGee et al., 2013). Instead, the AVF basalts resemble the FOZO or C isotopic mantle endmember (Hart et al., 1992; Hanan and Graham, 1996) closely overlapping with, or similar to, the compositional range of basalts from the Antarctic Peninsula, Victoria Land, and Balleny and Scott Islands

(Finn et al., 2005). The AVF also overlaps basalts from Australia and Tasmania that generally have a lower $^{206}Pb/^{204}Pb$ compared to New Zealand (Finn et al., 2005).

Prior studies have asserted that the isotopic Zealandia-Antarctic domain relates to the break-up of Gondwana at ~90 m.y. (e.g. Park et al., 2019). The Auckland volcanic field's $^{3}He/^{4}He$ signature of ~7 is commonly observed throughout the Zealandia-Antarctic domain (Fig. 9; e.g. Hoke et al., 2000; Nardini et al., 2009), and is similar to $^{3}He/^{4}He$ ratios along the Pacific-Antarctic Ridge (Moreira et al., 2008), parts of south-west Indian Ridge (SWIR) and in the 180 Ma Karoo flood basalt province (Georgen et al., 2003; Heinonen & Kurz, 2015). This low (~7 R_A) $^{3}He/^{4}He$ feature therefore stretches far beyond the region affected by the 90 m.y. breakup of Gondwana.

The homogeneity of the $^{3}He/^{4}He$ signature of the AVF compared to other isotopic and geochemical tracers (e.g. Pb isotopes and La/Yb ratios; McGee et al., 2013) raises the broader questions about possible "decoupling" of He isotopes. The preservation of isotopic heterogeneity in the mantle depends largely on the size of the heterogeneities, their rheological properties, and the time-scales of convective folding and mixing (Albarede, 2005). Preservation of Sr-Pb isotopic heterogeneity in the AVF (McGee et al., 2013; 2015), even within individual volcanic eruptions (McGee et al., 2015), implies a mantle mixing scenario similar to the S-Y-S (small- young- solid state) model of mantle heterogeneity proposed by Zindler et al. (1979) to account for the Nd isotopic variability in Reykjanes Peninsula basalts of Iceland. Prior work in the Auckland Volcanic Field established a correlation of basalt geochemistry with volcano size, degree of melting, and source enrichment (McGee et al., 2013). Possible decoupling of He even for these small-scale features, might imply that small-scale heterogeneities embedded in the mantle dominate the helium budget during melting. Alternatively, relatively long homogenization times for helium may have allowed diffusive overprinting of the ambient mantle from the heterogeneities

(Hart, 2008). Although we cannot distinguish between these two scenarios, long homogenization times might be consistent with any association to the Karoo flood basalts and the broader Zealandia-Antarctic mantle domain.

5. CONCLUSIONS

Olivine phenocrysts in lava and tephra from eight different volcanic centres, representing the compositional diversity of basalts from the Auckland Volcanic Field, were analysed by crushing for $^{3}He/^{4}He$, and He and CO_2 abundance. The CO_2/He ratio, and in particular the CO_2 abundance, vary inversely with indicators of trace element enrichment such as $[La/Yb]_N$. The lower CO_2 abundance in smaller-degree partial melts is most reasonably explained by early vapour CO_2 saturation and volatile exsolution. The He abundance, in contrast, does not vary with with geochemical indicators of enrichment, possibly due to more rapid equilibration of trapped helium with the surrounding melt during magma ascent.

Isotopic results indicate a remarkably homogeneous $^{3}He/^{4}He$ ratio of 7.10±0.26 R_A despite its significant trace element and Pb-Nd-Sr isotopic variability that is controlled by variations in the degree of melting of a heterogeneous mantle source. While AVF subalkaline basalts carry a slight indication of a mild subduction-related metasomatism, this process is not evident in their $^{3}He/^{4}He$ ratios. AVF basalts resemble other mantle-derived magmas from the Zealandia-Antarctic mantle domain (Hoke et al., 2000; Nardini et al., 2009; Heinonen and Kurz, 2015). The predominance of $^{3}He/^{4}He$ ratios near 7 R_A over this large scale (Hoke et al., 2000; Nardini et al., 2009; Heinonen and Kurz, 2015) may have originated during superplume-driven break-up of Gondwana and the associated emplacement of the Karoo flood basalts at ~180 Ma.

ACKNOWLEDGMENTS

The helium isotope analyses at OSU were supported by the National Science Foundation though grants OCE15-58798 and 17-63255. Partial funding for Rowe was provided by University of Auckland Research and Study Leave support. The authors would also like to thank P. Wallace for access to his HFB_4 facility and L. Moore for discussions on volatiles in shrinkage bubbles.

REFERENCES

Albarede, F. 2005. The survival of mantle geochemical heterogeneities. In Earth's Deep Mantle: Structure, Composition, and Evolution, (eds) R.D. Van Der Hilst, J.D. Bass, J. Matas, J. Trampert. Geophysical Monograph Series, 160. doi 10.1029/160GM04.

Aster, E.M., Wallace, P.J., Moore, L.R., Watkins, J., Gazel, E., Bodnar, R.J. 2016. Reconstructing CO_2 concentrations in basaltic melt inclusions using Raman analysis of vapour bubbles. Journal of Volcanology and Geothermal Research, 323, 148-162.

Brenna, M., Cronin, S.J., Smith, I.E.M., Tollan, P.M.E., Scott, J.M., Prior, D.J., Bambery, K., Ukstins, I.A. Olivine xenocryst diffusion reveals rapid monogentic basaltic magma ascent following complex storage at Pupuke Maar, Auckland Volcanic Field, New Zealand. Earth and Planetary Science Letters, 499, 13-22.

Coote, A. Shane, P., Fu, B. 2019. Olivine phenocryst origins and mantle magma sources for monogenetic basalt volcanoes in northern New Zealand from textural, geochemical and δ18O isotope data. Lithos, 344-345, 232-246.

Dunai, T., Porcelli, D., 2002. Storage and transport of noble gases in the subcontinental lithosphere, in: Porcelli, D., Wieler, R., Ballentine, C.J. (Eds.), Noble Gases in Geochemistry and Cosmochemistry. Mineral. Soc. Amer., Washington, D.C., pp. 371-409.

Finn, C.A., Muller, R.D., Panter, K.S. 2005. A Cenozoic diffuse alkaline magmatic province (DAMP) in the southwest Pacific without rift or plume origin. Geochemistry, Geophysics, Geosystems, 6 (1), doi: 10.1029/2004GC000723.

Gautheron, C., Moreira, M. 2002. He signature of the subcontinental lithospheric mantle. Earth and Planetary Science Letters, 199, 39-47.

Georgen, J.E., Kurz, M.D., Dick, H.J.B, Lin, J. 2003. Low 3He/4He ratios in basalt glasses from the western Southwest Indian Ridge (10°-24°E). Earth and Planetary Science Letters, 206, 509-528.

Gonnermann, H. M., Mukhopadhyay, S. 2007. Non-equilibrium degassing and a primordial source for helium in ocean-island volcanism. Nature, 449, doi:10.1038/nature06240

Graham, D.W. 2002. Noble gas isotope geochemistry of mid-ocean ridge and ocean island basalts: Characterization of mantle source reservoirs. In: Noble Gases in Geochemistry and

Cosmochemistry (eds D. Porcelli, C.J. Ballentine, and R. Wieler). Reviews in Mineralogy and Geochemistry, 47, 274-318.

Graham, D.W., Humphris, S.E., Jenkins, W.J., Kurz, M.D. 1992. Helium isotope geochemistry of some volcanic rocks from Saint Helena. Earth and Planetary Science Letters, 110, 121-131.

Graham, D.W., Hanan, B.B., Hémond, C., Blichert-Toft, J., Albarède, F., 2014. Helium isotopic textures in Earth's upper mantle. Geochem. Geophys. Geosyst. 15, 2048-2074.

Graham, D.W., Michael, P.J., Rubin, K.H. 2018. An investigation of mid-ocean ridge degassing using He, CO_2, and $\delta^{13}C$ variations during the 2005-06 eruption at 9°50'N on the East Pacific Rise. Earth and Planetary Science Letters, 504, 84-93.

Hanan, B.B., Graham, D.W. 1996. Lead and helium isotope evidence from oceanic basalts from a common deep source of mantle plumes. Science, 272 (5264), 991-995.

Hanyu, T., Kaneoka, I. 1997. The uniform and low 3He/4He ratios of HIMU basalts as evidence for their origin as recycled materials. Nature, 390, 273-276.

Hanyu, T., Kawabata, H., Tatsumi, Y., Kimura, J-I., Hyodo, H., Sato, K., Miyazaki, Chang, Q., Hirahara, Y., Takahashi, T., Senda, R., Nakai, S. 2014. Isotope evolution in the HIMU reservoir beneath St. Helena: implications for the mantle recycling of U and Th. Geochimica et Cosmochimica Acta 143, 232-252.

Hart, S.R., Hauri, E.H., Oschmann, L.A., Whitehead, J.A. 1992. Mantle plumes and entrainment: isotopic evidence. Science, 256 (5056), 517-520.

Hart, S.R., Kurz, M.D., Wang, Z. 2008. Scale length of mantle heterogeneities: constraints from helium diffusion. Earth and Planetary Science Letters, 269, 507-516.

Haase, K.M., Renno, A.D. 2008. Variation of magma generation and mantle sources during continental rifting observed in Cenozoic lavas from the Eger Rift, Central Europe. Chemical Geology 257, 192-202.

Heinonen, J.S., Kurz, M.D. 2015. Low-3He/4He sublithospheric mantle source for the most magnesian magmas of the Karoo large igneous province. Earth and Planetary Science Letters, 426, 305-315.

Hidas, K., Guzmics, T., Szabo, C., Kovacs, I., Bodnar, R.J., Zajacz, Z., Nedli, Z., Vaccari, L., Perucchi, A. 2010. Coexisting silicate melt inclusions and H2O-bearing, CO2-rich fluid inclusions in mantle peridotite xenoliths from the Carpathian-Pannonian region (central Hungary). Chemical Geology 274, 1-18.

Hilton, D.R., Fischer, T.P., Marty, B. 2002. Noble gases and volatile recycling at subduction zones. Reviews in mineralogy and geochemistry, 47, 319-370.

Hodder, A.P.W. 1984. Late Cenozoic rift development and intra-plate volcanism in northern New Zealand inferred from geochemical discrimination diagrams. Tectonphysics, 101, 293-318.

Hoke, L., Poreda, R., Reay, A., Weaver, S.D. 2000. The subcontinental mantle beneath southern New Zealand, characterised by helium isotopes in intraplate basalts and gas-rich springs. Geochimica et Cosmochimica Acta, 64 (14) 2489-2507.

Horspool, N.A., Savage, M.K., Bannister, S. 2006. Implications for intraplate volcanism and back-arc deformation in northwestern New Zealand, from joint inversion of receiver functions and surface waves. Geophysical Journal International, 166, 1466-1483.

Hopkins J.L., Timm, C., Millet, M-A., Poirier, A., Wilson, C.J.N., Leonard, G.S. 2016. Os isotopic constraints on crustal contamination in Auckland Volcanic Field basalts, New Zealand. Chemical Geology, 439, 83-97.

Horton, F., Farley, K., Jackson, M. 2019. Helium distributions in ocean island basalt olivines revealed by X-ray computed tomography and single-grain crushing experiments. Geochimica et Cosmochimica Acta, 244, 467-477.

Huang, Y., Hawkesworth, C., Smith, I., van Calsteren, P., Black, P. 2000. Geochemistry of late Cenozoic basaltic volcanism in Northland and Coromandel, New Zealand: implications or mantle enrichment processes. Chemical Geology, 164, 219-238.

Jiao, R., Seward, D., Little, A., Kohn, B.P. 2014. Thermal history and exhumation of basement rocks from Mesozoic to Cenozoic subduction cycles, central North Island, New Zealand. Tectonics, 33, 1920-1935.

Johnson, D. M., Hooper, P. R. & Conrey, R. M. (1999). XRF analysis of rocks and minerals for major and trace elements on a single low dilution Li-tetraborate fused bead. Advances in X-ray Analysis 41, 843-867.

Johnson, E.R., Wallace, P.J., Cashman, K.V., Granados, H.D., Kent, A.J.R. 2008. Magmatic volatile contents and degassing-induced crystallization at Volcan Jorullo, Mexico: Implications for melt evolution and the plumbing systems of monogenetic volcanoes. Earth and Planetary Science Letters 269, 478-487.

Knaack, C., Cornelius, S. B. & Hooper, P. R. (1994).Trace element analyses of rocks and minerals by ICP-MS. Technical Notes, GeoAnalytical Lab,Washington State University.

Kurz, M.D., Jenkins, W.J., Hart, S.R., 1982. Helium isotopic systematics of oceanic islands and mantle heterogeneity. Nature, 297, 43-47.

Leonard, G.S., Calvert, A.T., Hopkins, J.L., Wilson, C.J.N., Smid, E.R., Lindsay, J.M., Campion D,E. 2017. High-precision 40Ar/39Ar dating of Quaternary basalts from Auckland Volcanic Field, New Zealand, with implications for eruption rates and paleomagnetic correlations. Journal of Volcanology and Geothermal Research, 343, 60-74.

McCoy-West, A.J., Baker, J.A., Faure, K., Wysoczanski, R. 2010. Petrogenesis and origins of mid-Cretaceous continental intraplate volcanism in Marlborough, New Zealand: Implications for the long-lived HIMU magmatic mega-province of the SW Pacific. Journal of Petrology, 51 (10), 2003-2045.

McDonough, W.F., Sun, S.-s. 1995. The composition of the Earth. Chemical Geology, 120, 223-253.

McGee, L. 2012. Melting processes in small volume basaltic systems: the Auckland Volcanic Field, New Zealand. PhD Thesis, University of Auckland.

McGee, L.E., Millet, M.-A., Smith, I.E.M., Nemeth, K., Lindsay, J.M. 2012. The inception and progression of melting in a monogenetic eruption: Motukorea Volcano, the Auckland Volcanic Field, New Zealand. Lithos 155, 360-374.

McGee, L.E., Smith, I.E.M. 2016. Interpreting chemical compositions of small scale basaltic sytems: A review. Journal of volcanology and Geothermal Research, 325, 45-60.

McGee, L., Smith, I.E.M., Millet, M-A., Handley, H.K., Lindsay, J.M. 2013. Asthenospheric control of melting processes in a monogenetic basaltic system: a case study of the Auckland Volcanic Field, New Zealand. Journal of Petrology, 54 (10), 2125-2153.

McGee, L.E., Millet, M-A., Beier, C., Smith, I.E.M., Lindsay, J.M. 2015. Mantle heterogeneity controls on small-volume basaltic volcanism. Geology, 43 (6), 551-554.

Moore, L.R., Gazel, E., Tuohy, R., Lloyd, A.S., Esposito, R., Steele-MacInnis, M, Hauri, E.H., Wallace, P.J., Plank, T., Bodnar, R.J. 2015. Bubbles matter: assessment of the contribution of vapour bubbles to melt inclusion volatile budgets. American Mineralogist, 100, 806-823.

Nardini, I., Armienti, P., Rocchi, S., Dallai, L., Harrison, D. 2009. Sr-Nd-Pb-He-O isotope and geochemical constraints on the genesis of Cenozoic magmas from the West Antarctic Rift. Journal of Petrology, 50 (7), 1359-1375.

Nichols, A.R.L., Wysoczanski, R.J., Tani, K., Tamura, Y., Baker, J.A., Tasumi, Y. 2012. Melt inclusions reveal geochemical cross-arc variations and diversity within magma chambers feeding the Higashi-Izu Monogenetic Volcano Field, Izu Peninsula, Japan. Geochemistry, Geophysics, Geosystems, 13 (9), 10/1029/2012GC004222.

Panter, K.S., Blusztajn, J., Hart, S.R., Kyle, P.R., Esser, R., McIntosh, W.C. 2006. The origin of HIMU in the SW Pacific: Evidence from Intraplate Volcanism in the Southern New Zealand and Subantarctic Islands. Journal of Petrology, 47 (9), 1673-1704.

Patterson, D.B., Honda, M., McDougall, I. 1994. Nobel gases in mafic phenocrysts and xenoliths from New Zealand. Geochimica et Cosmochimica Acta, 58 (20), 4411-4427.

Park, S-H., Langmuir, C.H., Sims, K.W.W., Blichert-Toft, J., Kim, S.S., Scott, S.R., Lin, J., Choi, H., Yang, Y-S., Michael, P.J. 2019. An isotopically distinct Zealandia-Antarctic mantle domain in the Southern Ocean. Nature Geoscience, 12, 206-214.

Porcelli, D.R., O'Nions, R.K., Galer, S.J.G., Cohen, A.S., Mattey, D.P., 1992. Isotopic relationships of volatile and lithophile trace elements in continental ultramafic xenoliths. Contributions to Mineralogy and Petrology, 110, 528-538.

Poreda, R., Craig, H., 1989. Helium isotope ratios in circum-Pacific volcanic arcs. Nature 338, 473-478.

Rasoazanamparany, C., Widom, E., Valentine, G.A., Smith, E.I., Cortes, J.A., Kuentz, D., Johnsen, R. 2015. Origin of chemical and isotopic heterogeneity in a mafic, monogenetic volcanic field: A case study of the Lunar Crater Volcanic Field, Nevada. Chemical Geology, 397, 76-93.

Reid, M.R., Graham, D.W. 1996. Resolving lithospheric and sub-lithospheric contributions to helium isotope variations in basalts from the southwestern US. Earth and Planetary Science Letters. 144, 213-222.

Reiners, P.W. 1998. Reactive melt transport in the mantle and geochemical signatures of mantle-derived magmas. Journal of Petrology, 39 (5) 1039-1061.

Scott, J.M., Waight, T.E., van der Meer, Q.H.A., Palin, J.M., Cooper, A.F., Munker, C. 2014. Metasomatized ancient lithospheric mantle beneath the young Zealandia microcontinent and

its role in HIMU-like intraplate magmatism. Geochemistry, Geophysics, Geosystems, 15, 10.1002/2014GC005300.

Seebeck, H., Nicol, A. Giba, M., Pettinga, J., Walsh, J. 2014. Geometry of the subducting Pacific plate since 20 Ma, Hikurangi margin, New Zealand. Journal of the Geological Society, London. 171, 131-143.

Smith, I.E.M., Okado, T., Itaya, T., Black, P.M. 1993. Age relationships and tectonic implications of late Cenozoic basaltic volcanism in Northland, New Zealand. New Zealand Journal of Geology and Geophysics, 36 (3), 385-393.

Stracke, A., Bourdon, B. 2009. The importance of melt extraction for tracing mantle heterogeneity. Geochimica et Cosmochimica Acta, 73, 218-238.

Strong, M., Wolff, J. 2003. Compositional variations within scoria cones. Geology, 31, 143-146.

Sun, S.-s., McDonough, W.F. 1989. Chemical and isotopic systematics of oceanic basalts: implications for mantle composition and processes. Geological Society of London, Special Publications, 42, 313-345.

Tucker, J.M., Mukhopadhyay, S., Gonnermann, H.M. 2018. Reconstructing mantle carbon and noble gas contents from degassed mid-ocean ridge basalts. Earth and Planetary Science Letters, 496, 108-119.

Tucker, J.M., Hauri, E.H., Pietruszka, A.J., Garcia, M.O., Marske, J.P., Trusdell, F.A. 2019. A high carbon content of the Hawaiian mantle from olivine-hosted melt inclusions. Geochimica et Cosmochimica Acta, 254, 156-172.

Woodhead, J.D. 1996. Extreme HIMU in an oceanic setting: the geochemistry of Mangaia Island (Polynesia), and temporal evolution of the Cook-Austral hotspot. Journal of Volcanology and Geothermal Research, 72, 1-19.

Zindler, A., Hart, S.R., Frey, F.A., Jakobsson, S.P. 1979. Nd and Sr isotope ratios and rare earth element abundances in Reykjanes Peninsula basalts evidence for mantle heterogeneity beneath Iceland. Earth and Planetary Science Letters, 45, 249-262.

FIGURE CAPTIONS

Figure 1: Map of the Auckland Volcanic Field vent sites. Red stars indicate volcanoes analysed in this study.

Figure 2: Microscope images of sample AU59337, Rangitoto subalkaline tephra, before (A) and after (B) HBF_4 treatment.

Figure 3: Whole rock rare earth element (A) and trace element (B) distributions in tephras and lavas (data from this study and McGee, 2012) normalized to C1 chondrite and primitive mantle, respectively (Sun and McDonough, 1989; McDonough and Sun, 1995). (C)

Chondrite normalized REE ratios used for classification as in text, subdivided into alkaline and subalkaline compositions, with alkaline magmas categorized based on $La/Yb_{[N]}$. Shading, from light grey, to dark grey, to black corresponds with increase LREE and MREE enrichment for low-, transitional-, and high-alkali enriched basalts.

Figure 4: $^{3}He/^{4}He$ (R/R_A) for AVF olivine versus olivine trapped He content (cm^3 STP/g).

Figure 5: Comparison between (A) $^{3}He/^{4}He$ (R/R_A, where R is the measured ratio and R_A is the atmospheric value of $1.39x10^{-6}$), and (B) He (cm^3 STP/g) for HFB4-treated Rangitoto olivine and comparable "glassy" subalkaline (black circle), alkaline (black star) tephra, and subalkaline lava (open star). Also plotted is a comparison between Maungarei lava and tephra olivine separates (open square). Error bars are 2s.

Figure 6: Whole rock trace element abundances versus (a-b) He abundances and (c-f) CO_2 abundances. Note that the Lake Pupuke sample is predominantly composed of xenocrystic olivine but for the purposes of this study, gas chemistry from olivine is plotted versus its whole rock composition.

Figure 7: Chondrite Normalized (McDonough and Sun, 1995) whole rock La/Yb versus (A) $^{3}He/^{4}He$, (B) trapped He content of olivine, (C) trapped CO_2 content of olivine, and (D) $CO_2/^{3}He$. Error bars for La/Yb are included in panel (A). Long and short dashed lines in (A) represent the average (long-dash) and 1std dev (short dash) for AVF phenocrysts. The light grey diamond represents a potential xenocrystic sample (Lake Pupuke; Brenna et al., 2018), however is plotted based on whole rock $La/Yb_{[N]}$. Symbols and shading are the same as in Fig. 3.

Figure 8: Schematic diagram demonstrating the effect of varying degree of mantle partial melting on early CO_2 vapour saturation and resulting early saturation of CO_2-rich vapour, resulting in high incompatible trace element (ICE)/CO_2 ratios compared to higher degree

partial melts. Also illustrated is a conceptual diagram for the potential impact of ascent rate (slow versus fast) on diffusion and re-equilibration between melt inclusions and shrinkage bubbles and the likely impact on measured olivine CO_2/He. See the text for a detailed explanation of melt inclusion re-equilibration potential.

Figure 9: $^3He/^4He$ (R/R_A) for New Zealand basalts and mantle xenoliths. Data from this study indicated by red triangles. Literature data for the Taupo Volcanic Zone (TVZ), South Island basalts and xenoliths, Northland, and the AVF in black (Patterson et al, 1994; Hoke et al., 2000).

Figure 1

Click here to download high resolution image

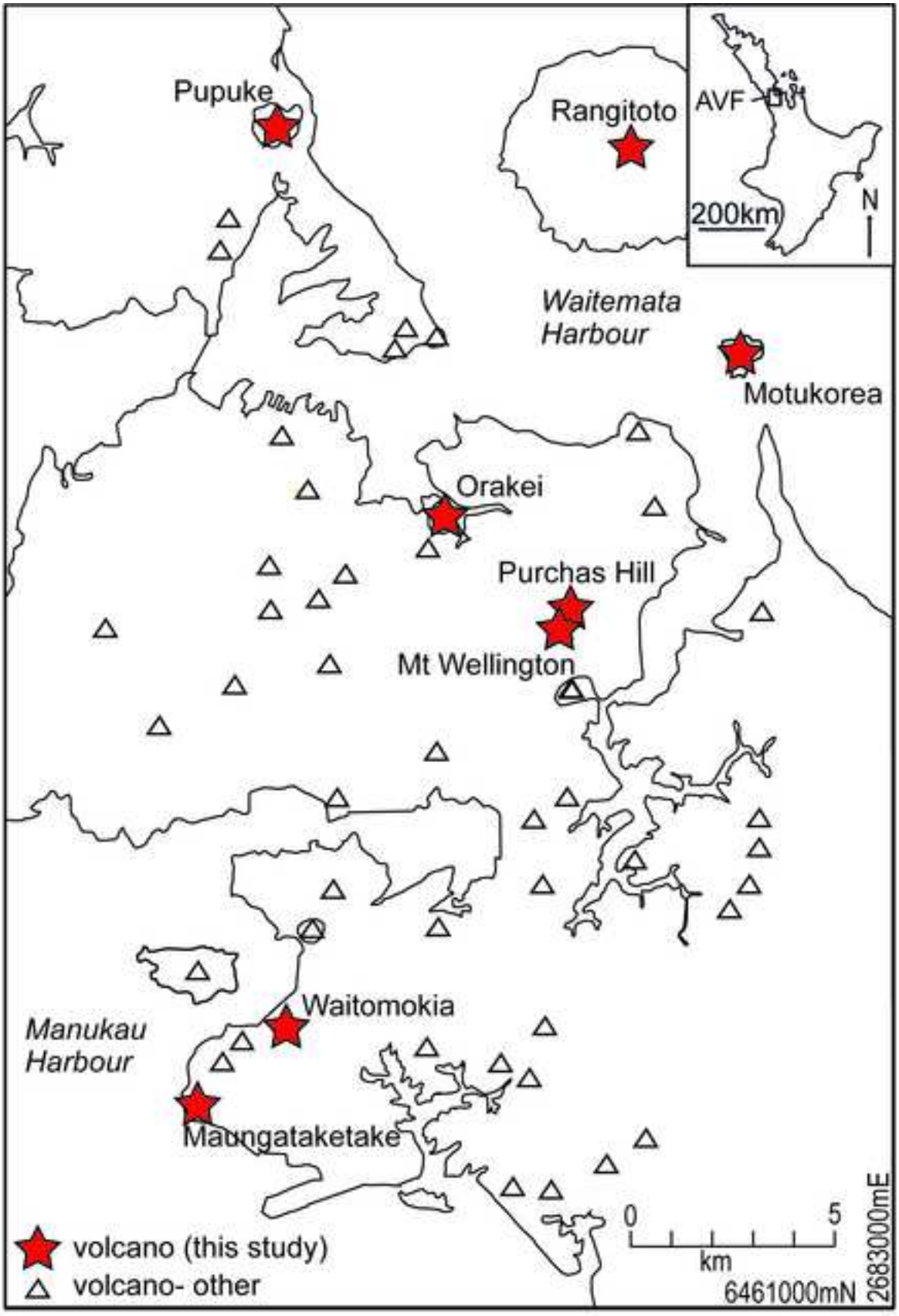

Figure 1

Figure 2

Click here to download high resolution image

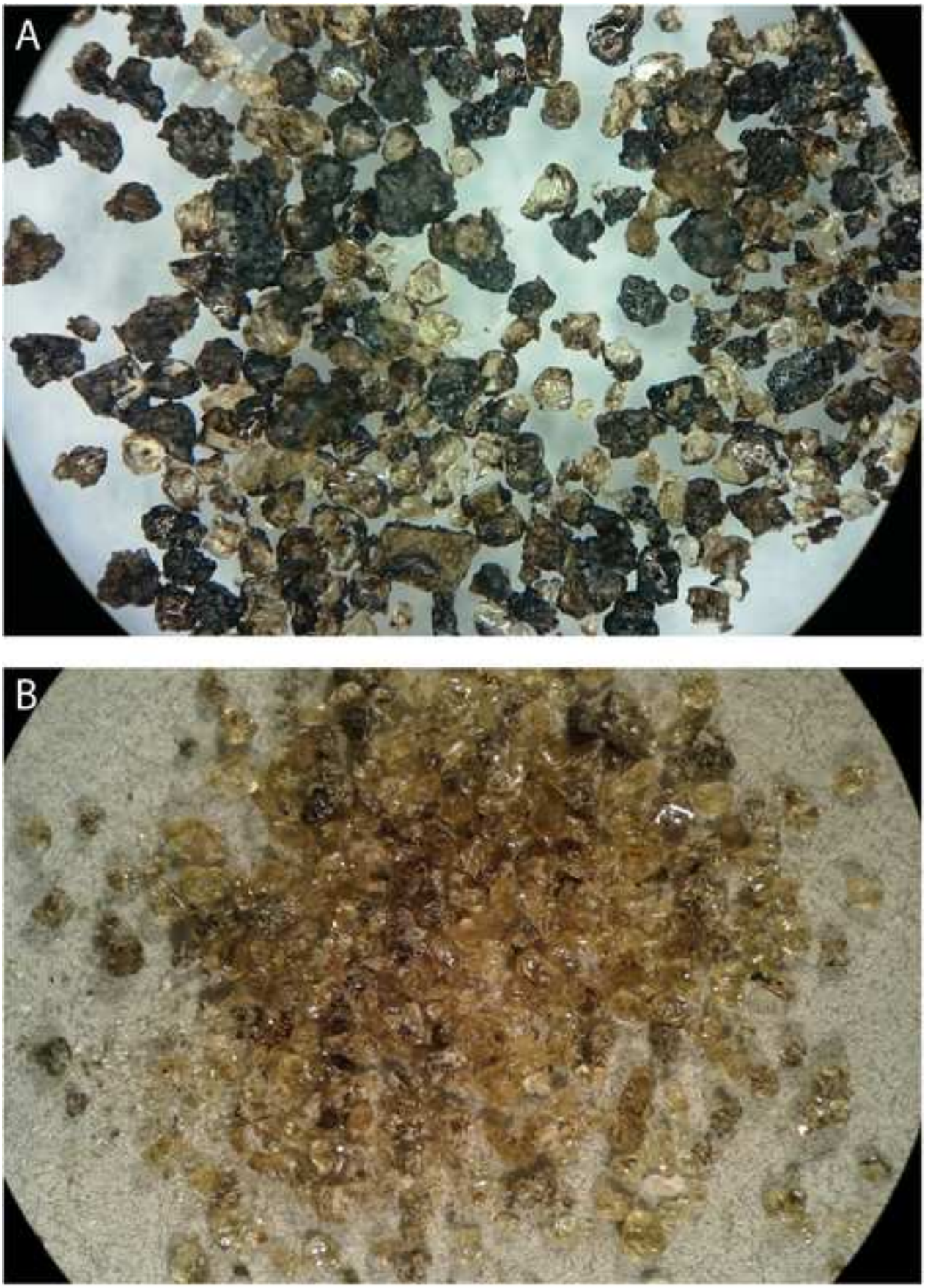

Figure 2

Figure 3

Click here to download high resolution image

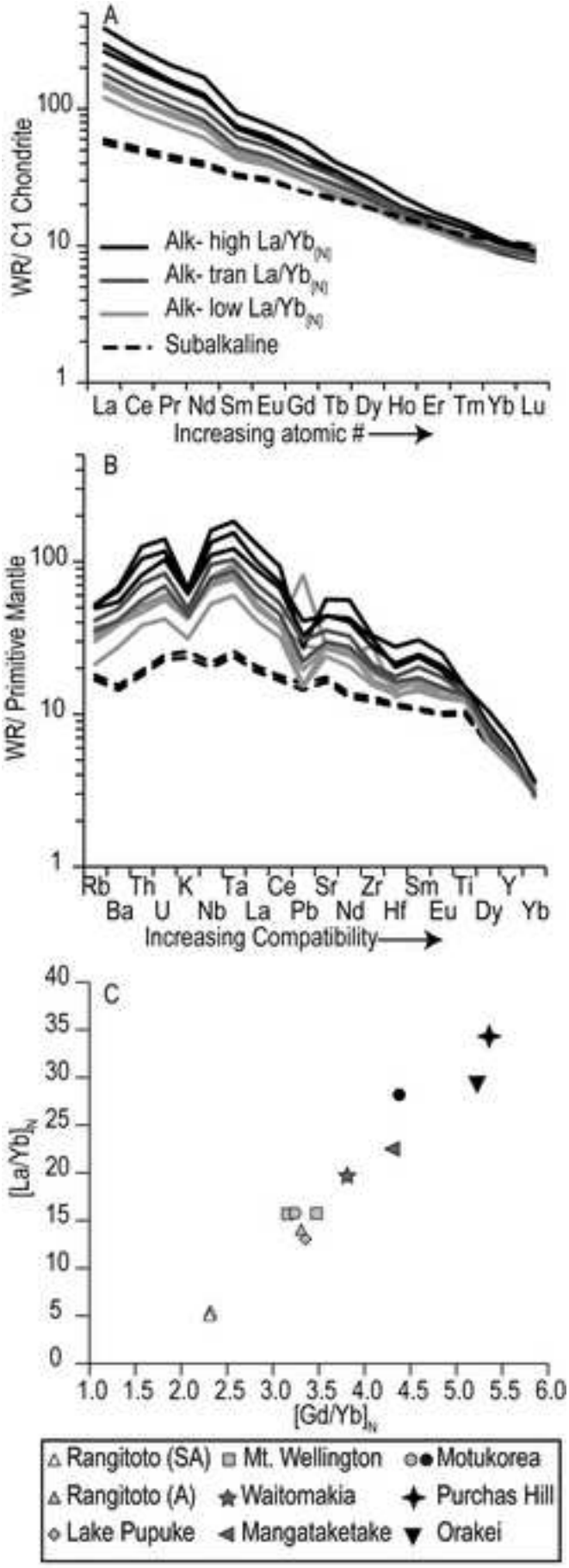

Figure 3

Figure 4

Click here to download high resolution image

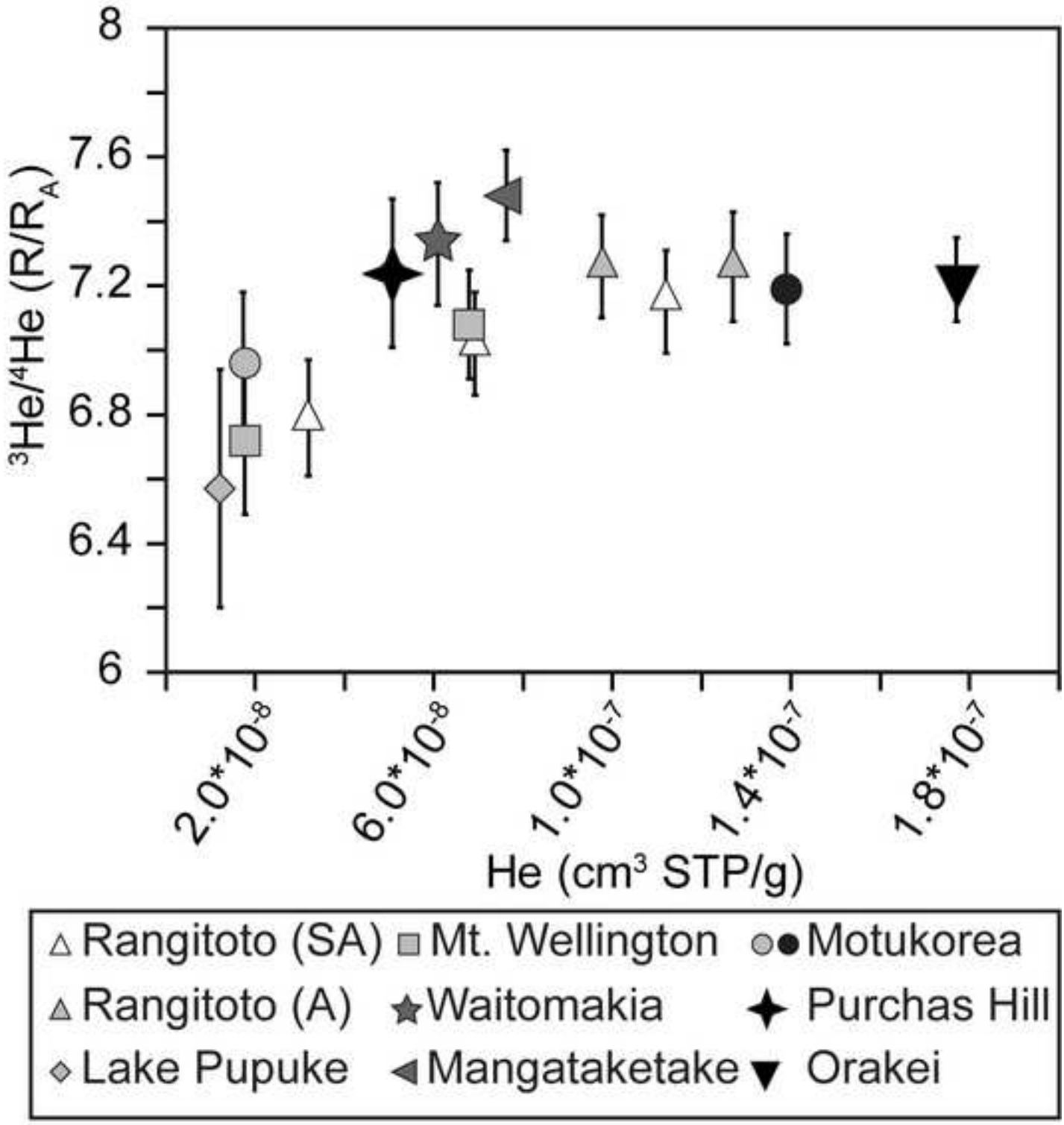

Figure 4

Figure 5

Click here to download high resolution image

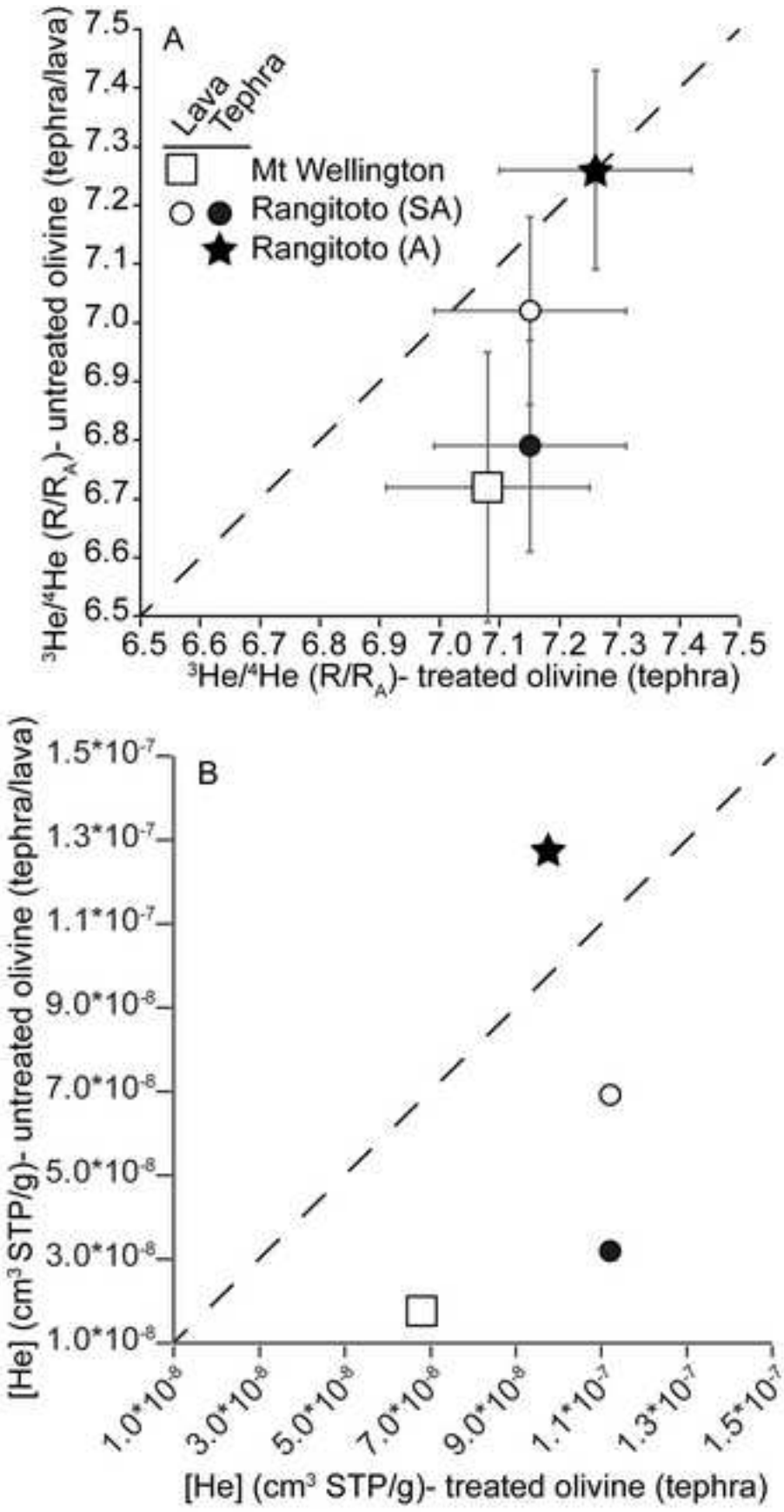

Figure 5

Figure 6

Click here to download high resolution image

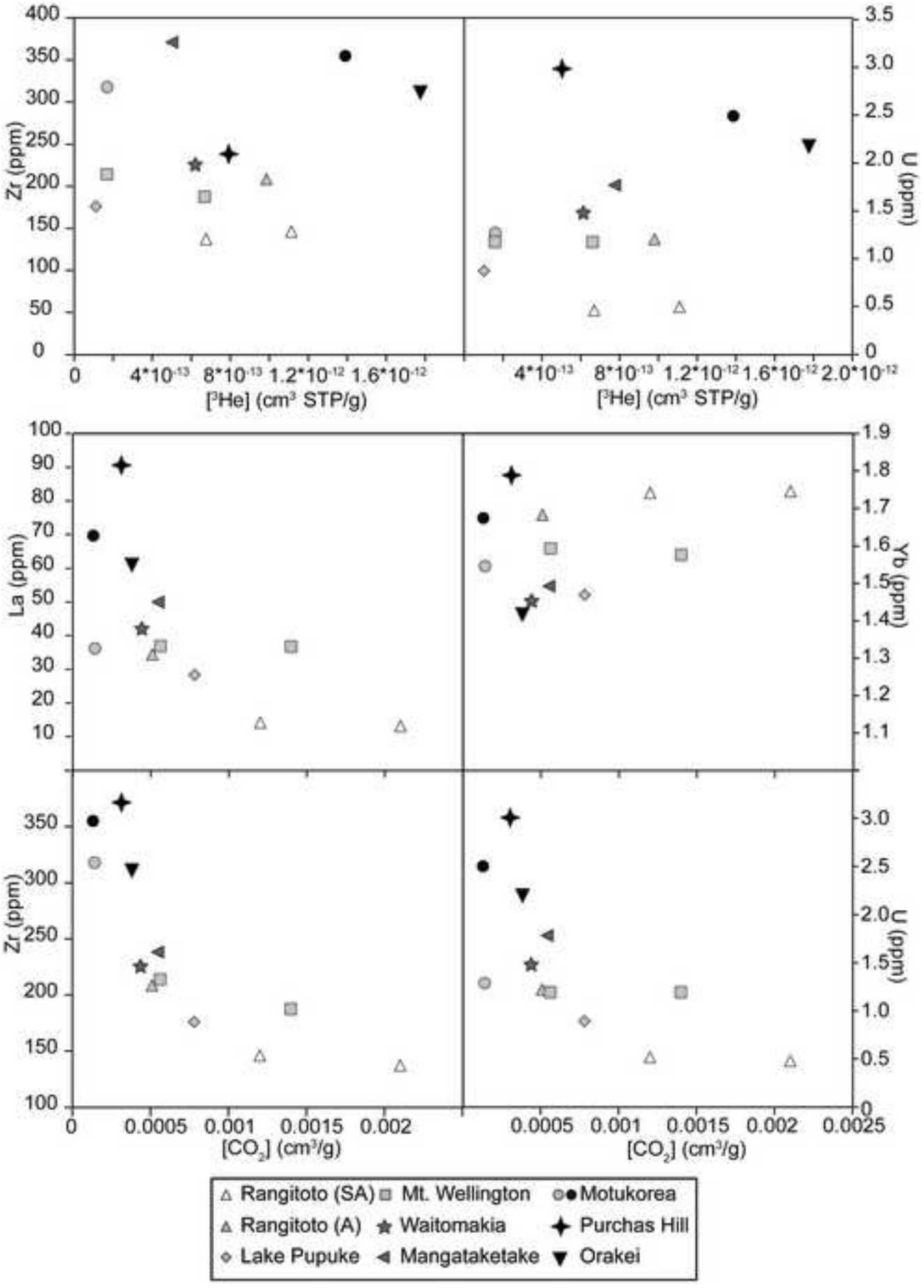

Figure 6

Figure 7
Click here to download high resolution image

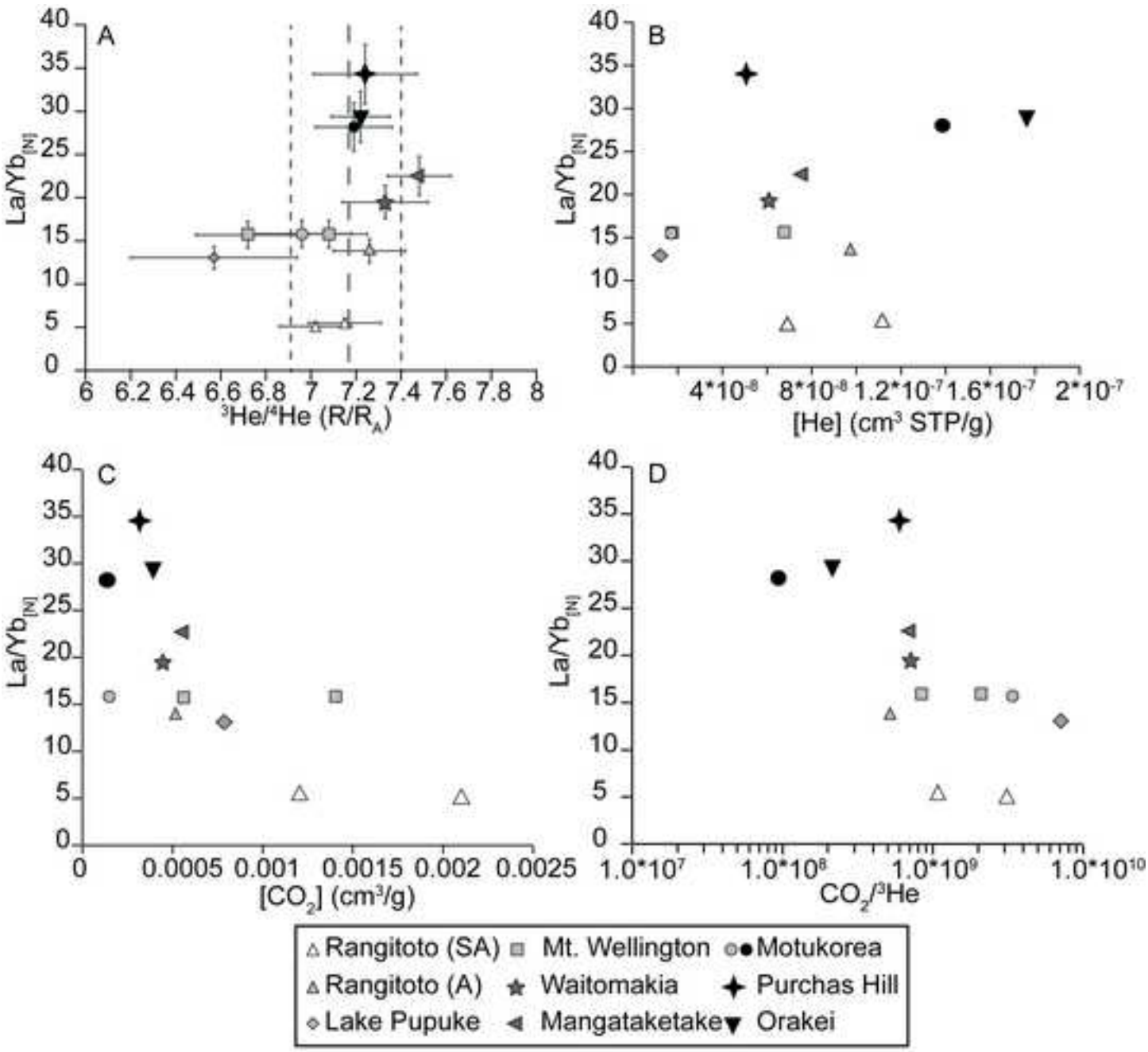

Figure 7

Figure 8

Click here to download high resolution image

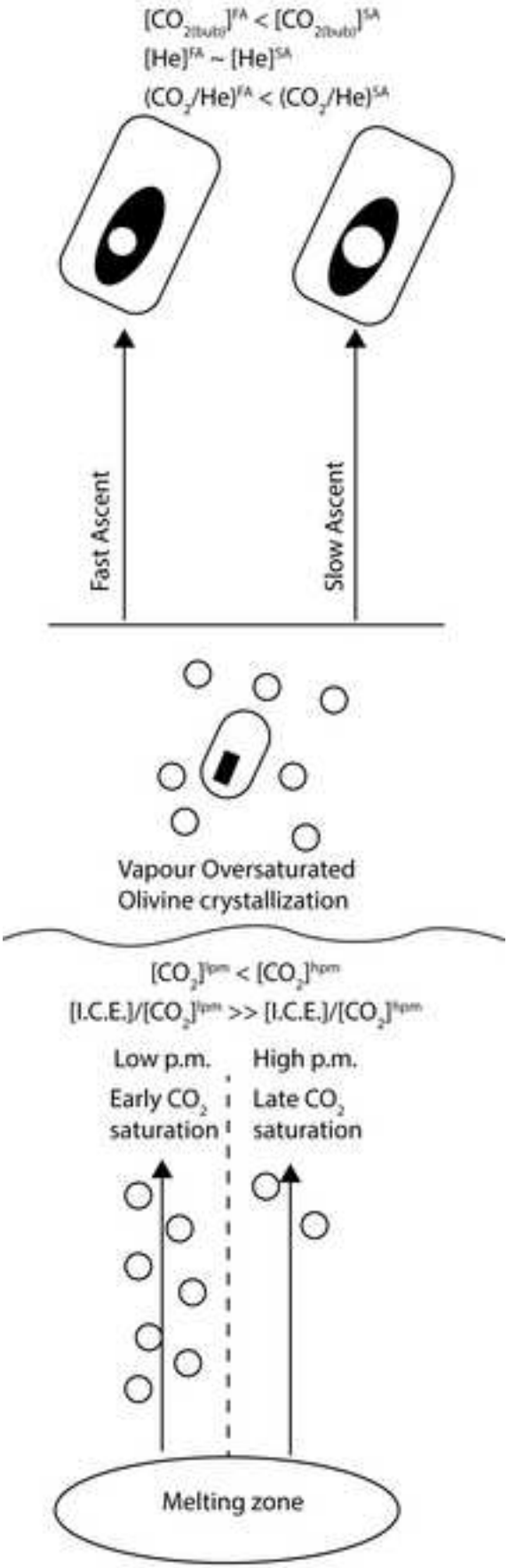

Figure 8

Figure 9

Click here to download high resolution image

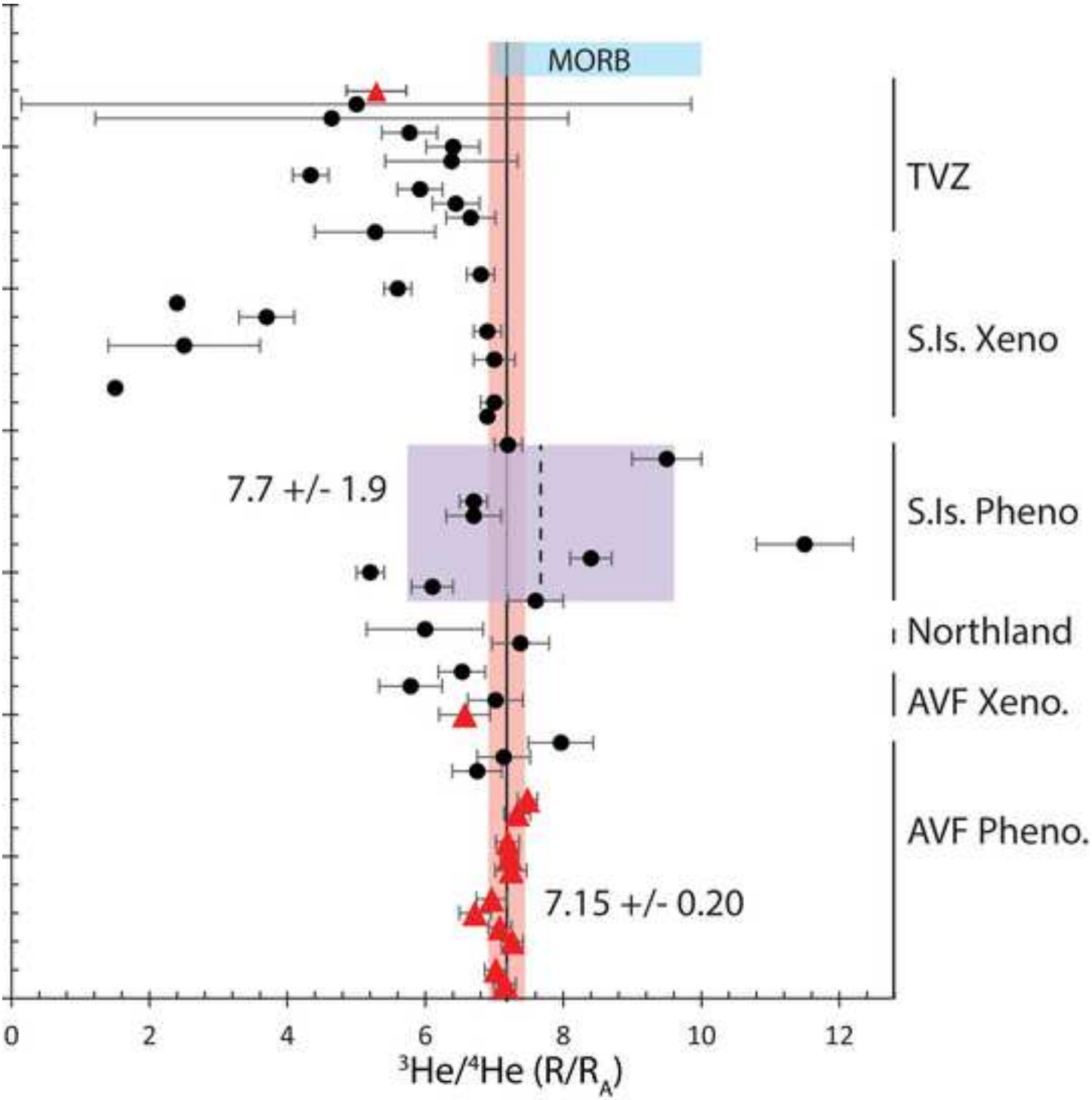

Figure 9

Table

Click here to download Table: Table 1.xlsx

Table 1: Sample major element and trace element composition.

Location	Rangitoto	Rangitoto	Rangitoto	Rangitoto	Rangitoto	Lake Pupuke	Maungarei
Sample ID	AU59337-1	AU59337-2	MR-Rangi1	AU49951-1	AU49951-2	Pupuke7	078
Age (ka)	0.504	0.504	0.504	0.553	0.553	193	10.3
Type	T	T	L	T	T	T	T
HBF4	N	Y	N	N	Y	N	Y
Class	SA	SA	SA	A-low	A-low	A-low	A-low
Normalized Major Elements (Weight %):							
SiO2	49.45		49.46	47.76		46.26	44.17
TiO2	2.111		2.013	2.734		2.458	2.597
Al2O3	15.12		14.71	14.42		13.30	12.71
FeO*	11.35		11.53	11.64		13.34	12.85
MnO	0.167		0.168	0.175		0.185	0.193
MgO	7.95		8.55	6.93		10.39	12.10
CaO	9.49		9.38	10.76		9.58	10.60
Na2O	3.32		3.24	3.70		3.10	2.93
K2O	0.75		0.68	1.35		0.91	1.27
P2O5	0.291		0.271	0.529		0.481	0.580
Sum	99.84		100.29	98.32		99.08	99.17
LOI %	0.00		0.00	1.04		0.72	0.52
Trace element abundances (ppm)							
La	14.17		13.16	34.38		28.36	36.74
Ce	31.80		29.86	67.66		57.02	69.49
Pr	4.24		3.96	8.24		6.93	8.70
Nd	18.57		17.44	33.24		28.12	34.73
Sm	4.88		4.72	7.35		6.33	7.27
Eu	1.72		1.66	2.41		2.16	2.45
Gd	4.96		4.95	6.83		6.05	6.76
Tb	0.81		0.78	1.03		0.90	0.98
Dy	4.63		4.68	5.61		4.93	5.42
Ho	0.88		0.86	0.97		0.87	0.95
Er	2.19		2.19	2.33		2.04	2.24
Tm	0.29		0.29	0.30		0.25	0.28
Yb	1.74		1.75	1.68		1.47	1.58
Lu	0.25		0.25	0.24		0.20	0.23
Ba	109		101	280		195	274
Th	1.65		1.53	4.49		3.27	3.98
Nb	15.61		14.50	52.59		38.34	49.91
Y	21.57		21.32	24.25		21.04	23.67
Hf	3.63		3.48	5.00		4.18	4.46
Ta	1.07		0.99	3.35		2.49	3.19
U	0.52		0.48	1.22		0.89	1.19
Pb	2.94		2.69	3.65		2.80	15.30
Rb	11.5		10.8	23.8		13.7	20.7
Cs	0.43		0.41	0.62		0.27	0.35
Sr	371		348	583		510	602
Sc	24.7		24.9	24.3		21.8	23.3
Zr	146		137	209		176	188

Notes: 1Compositions from McGee (2012). Type T (tephra) and L (lava). Basalts are classifed subalkaline/a

Table 2

Click here to download Table: Table 2-DG.xlsx

Table 2: He isotopic composition and CO_2 and He abundances in olivine.

Sample ID	Mass (g)	$^3He/^4He$ (R/R_A)	2-sigma	[He] (cm^3 STP/g)	[CO_2] (cm^3 STP/g)	$CO_2/^3He$
AU59337-1	0.4333	6.79	0.18	3.19E-08		
AU59337-2	0.1012	7.15	0.16	1.12E-07	0.0012	1.08E+09
MR-Rangi1	0.1747	7.02	0.16	6.92E-08	0.0021	3.11E+09
AU49951-1	0.1255	7.26	0.17	1.27E-07		
AU49951-2	0.1081	7.26	0.16	9.76E-08	*0.00051*	5.18E+08
Pupuke7	0.1172	6.57	0.37	1.21E-08	0.00078	7.06E+09
078	0.1192	7.08	0.17	6.79E-08	0.0014	2.10E+09
AU62410	0.2763	6.72	0.23	1.77E-08	0.00056	3.39E+09
AU62444	0.2647	6.96	0.22	1.73E-08	*0.00014*	8.36E+08
AU62402	0.0887	7.24	0.23	5.07E-08	*0.00031*	6.08E+08
OB-16B-102m	0.1275	7.22	0.13	1.77E-07	*0.00038*	2.14E+08
AU62438	0.0709	7.19	0.17	1.39E-07	*0.00013*	9.36E+07
Waitomakia-Q	0.1438	7.33	0.19	6.09E-08	*0.00044*	7.09E+08
Mangataketake	0.2436	7.48	0.14	7.62E-08	0.00056	7.07E+08
Onga-1 (TVZ)	0.1780	5.27	0.52	2.81E-09	0.00051	2.48E+10

The $^3He/^4He$ ratio (R) is reported relative to the atmospheric ratio (R_A) of $1.39x10^{-6}$.

Italicized [CO_2] results indicate that the measured pCO_2 was < 1 mtorr.

Onga-1 is a basalt from the Taupo volcanic zone (TVZ) analyzed for comparision to the Auckland volcanic field l

***Declaration of Interest Statement**

Declaration of interests

☒ The authors declare that they have no known competing financial interests or personal relationships that could have appeared to influence the work reported in this paper.

☐The authors declare the following financial interests/personal relationships which may be considered as potential competing interests: